Korean J. Chem. Eng., 34(6), 1858-1866 (2017)
DOI: 10.1007/s11814-017-0047-8

pISSN: 0256-1115
eISSN: 1975-7220

Iron-manganese-magnesium mixed oxides catalysts for selective catalytic reduction of NO_x with NH_3

Kang Zhang*, Liting Xu*, Shengli Niu*, Chunmei Lu*,†, Dong Wang, Qi Zhang*, and Jing Li*****

*School of Energy and Power Engineering, Shandong University, Jinan 250061, China
**School of Environment, Tsinghua University, Beijing 100084, China
***School of Chemistry and Chemical Engineering, Shandong University, Jinan, Shandong 250100, China
(*Received 15 July 2016 • accepted 27 February 2017*)

Abstract−SCR activity at low temperature over iron oxide catalyst was prominently optimized by adding manganese and magnesium. $Fe_{0.7}Mn_{0.15}Mg_{0.15}O_z$(n(Mn)/[n(Fe)+n(Mn)+n(Mg)])=0.15 and n(Mg)/[n(Fe)+n(Mn)+n(Mg)]=0.15) presented better performance in the low temperature SCR and NO_x conversion of 90% could be achieved over 125 °C. Meanwhile, part of manganese and magnesium oxides were highly dispersed on the catalyst surface in an amorphous phase to react with iron oxide to form solid solution. Manganese and magnesium dopants could optimize the pore structure and distribution of γ-Fe_2O_3 to enhance the surface area and pore volume. Moreover, O_2 participated in SCR reaction at a faster rate than NH_3. In addition, the effect of SO_2 was proved to be irreversible, whereas the inhibition of H_2O could be rapidly removed after its removal.

Keywords: $Fe_{0.7}Mn_{0.15}Mg_{0.15}O_z$ Catalyst, γ-Fe_2O_3 Catalyst, Low-temperature SCR, H_2O and SO_2 Resistance, Catalyst Activity

INTRODUCTION

Nitrogen oxides (NO_x, normally includes NO, NO_2, and N_2O, etc.) emitted by coal combustion in power plants, contribute to air pollution for photochemical smog, ozone depletion, and global warming [1,2]. Selective catalytic reduction (SCR) of NO_x with ammonia (NH_3) has been well proved and widely used to eliminate NO_x in the flue gas from the stationary sources [3], which is generally described as Eq. (1).

$$4NH_3+4NO+O_2 \rightarrow 4N_2+6H_2O \quad (1)$$

As the core of SCR, catalysts are crucial to the efficient denitrification. At present, the typical commercial catalysts are the vanadium-based catalysts, such as V_2O_5-WO_3 mixed with WO_3 or MoO_3. However, restricted by a narrow activity temperature window from 300 °C to 400 °C, it is necessary to install SCR devices in the upstream of flue gas desulfurization unit, and the catalysts are susceptible to deactivation by dust deposition or SO_2 poisoning. Besides, this catalyst is also obviously restricted by the disadvantages of vanadium toxicity and high operating cost. Thus, it is very intense to explore new catalyst with high denitrification efficiency at low-temperature to be placed downstream of desulfurizer and precipitator in the power generation system [4].

Catalysts with transition metal oxide as active component have been demonstrated to gain potential to substitute the conventional V_2O_5-WO_3(MoO_3)/TiO_2 catalyst of manganese-based, cerium-based, copper-based or iron-based ones [5-7], which could present activity in the low- or medium-temperature SCR of NO_x with NH_3. Compared with the catalysts above, iron-based catalysts are prominent for their high activity, low cost and absence of toxicity. In a recent study, Fe_2O_3-TiO_2 catalyst prepared by Kato [8] gained high NO_x conversion of 90% and high N_2 selectivity from 350 °C to 450 °C. And other researchers prepared the Fe_2O_3/AC catalyst [9] and Fe_2O_3/ACF catalyst [10] using activated carbon and activated carbon fiber, respectively, whose NO_x conversion was fairly good under 200 °C. But the carbon based material would participate in the reaction, where the carbon based material itself is thus consumed. Because of the excellent performance of Fe_2O_3, we have used iron oxide as catalytic component in this study. Nevertheless, the temperature window of iron oxide catalyst is too high to meet the low-temperature SCR process. Therefore, we tried to modify the γ-Fe_2O_3 catalyst through doping transition metal elements in this study. According to the literature, manganese oxides shows excellent performance in the low-temperature SCR for the various types of labile oxygen, which has gained great promotion in the catalytic cycle. The activity at low temperature of the catalysts, which were based on the titania and loaded with several types of transition metal elements, was investigated by Peña [11], and the results showed that the order of the activity of all types metal elements was in the sequence of Mn, Cu, Cr, Co, Fe, V and Ni. Kapteijn [12] investigated the activity and selectivity of pure manganese oxides in SCR, and found that NO_x conversion was over 90% at 177 °C. Furthermore, Liu [13] doped different metal elements into $FeTiO_x$ catalyst and found that Mn was the optimal auxiliary element, which could increase the SCR activity at low temperature. However, the catalysts doped by Mn are susceptible to deactivation by SO_2 poisoning. Shen [14] found that adding a little SO_2 in the flue gas would make NO_x conversion decrease by 60%. Thus, to improve

†To whom correspondence should be addressed.
E-mail: cml@sdu.edu.cn
‡The paper will be reported in the 11th China-Korea Clean Energy Workshop.

the resistant to SO_2 of the catalysts, we tried to find another auxiliary that could improve the SO_2 resistant of the catalysts. According to Valanidou [15], Ag/MgO-CeO_2-Al_2O_3 catalyst for low-temperature SCR exhibited excellent activity and prominent resistance to SO_2 for the function of MgO. Therefore, we introduced the Mg element as another dopant.

We prepared SCR catalysts of $Fe_{0.7}Mn_{0.15}Mg_{0.15}O_z$ and γ-Fe_2O_3 through the co-precipitation method with ammonium hydroxide as the precipitant. The $Fe_{0.7}Mn_{0.15}Mg_{0.15}O_z$ catalyst was picked out in our previous study among a series of iron-manganese-magnesium mixed oxides catalysts. This study indicated that $Fe_{0.7}Mn_{0.15}Mg_{0.15}O_z$ activity in SCR at low temperature was significantly improved compared with γ-Fe_2O_3. We investigated the effects of O_2 and NH_3 on NO_x conversion, including the concentration influences and the transient response behaviors. Furthermore, the resistance to SO_2 and H_2O of the catalyst was also tested. Meanwhile, to explore the promotional mechanisms for SCR activity with the doping of manganese and magnesium, structure properties were demonstrated by X-ray diffraction (XRD), porous structures and pore size distribution were tested by N_2 adsorption-desorption, the microstructure were described by scanning electron microscope (SEM), and the surface component was characterized by energy dispersive spectrometer (EDS).

MATERIAL AND METHOD

1. The Preparation of Catalysts

SCR catalysts of $Fe_{0.7}Mn_{0.15}Mg_{0.15}O_z$ (where 0.15 represents the molar fraction of Mn/(Fe+Mn+Mg) or Mg/(Fe+Mn+Mg)) and γ-Fe_2O_3 were prepared by the co-precipitation method with $FeSO_4 \cdot 7H_2O$, $Mg(NO_3)_2 \cdot 6H_2O$ and $Mn(NO_3)_2$ solution (50%) used as precursors, and ammonium hydroxide being precipitator. First, the precursors were dissolved in the 250 mL distilled water to make a mixture solution where the total ion concentration of Fe^{3+}, Mn^{2+} and Mg^{2+} was 0.2 mol. And then the mixture solution was stirred for one hour. The next step was titrating the solution into the ammonium hydroxide solution of 2 mol/L until the PH was 9-10. Without aging, the turbid liquid was filtered and the precipitate was washed with distilled water several times to wash off the foreign ions. After these pretreatments, the precipitate was dipped and filtered with Na_2CO_3 solution of 1mol/L. Then, after handling by the method of microwave, the precursors were washed until the PH reached 7. And this was followed by drying in the drying oven at 105 °C for 12 hours and calcining at 400 °C for 5 hours. Finally, the calcined samples were crushed and sieved to 40-60 mesh for SCR performance tests.

2. Activity Measurement

SCR performance of the catalysts was tested in a quartz fixed-bed reactor. The reactor mainly consisted of three sections: gas supplying system, SCR reaction system and analyzer system. The catalyst powders were loaded into a vertical quartz tube and heated by a vertical fixed-bed reactor with a type K thermocouple, inserted directly into the quartz tube, controlling the reactor temperature. During activity test, the fed gas concentration of NO, NH_3 and O_2 was kept at 1,000 μL/L, 1,000 μL/L and 3.5%, respectively, with N_2 balance at the total flow rate of 2 L/min through 4 mL catalyst, which was corresponding to a gas hourly space velocity (GHSV) of 30000/h. The gas flow rates were controlled by mass flowmeters. The experiments with various concentrations of NH_3 and O_2 were obtained by adjusting the composing ratios of gas mixture with no change of the total flow rate. The transient response experiments were carried out by controlling the mass flowmeters. During all measurements, the concentration of NO_x, NH_3 and O_2 was monitored and exhibited by a flue gas analyzer (Optima7.0, York Instruments Co. Ltd., Germany). NO_x conversion (η) was calculated by the equation following:

$$\eta = \frac{[NO_x]_{in} - [NO_x]_{out}}{[NO_x]_{in}} \times 100\% \quad (2)$$

where $[NO_x]_{in}$ and the $[NO_x]_{out}$, respectively, represented the NO_x concentration at the inlet and the outlet of the reactor.

We also measured N_2 selectivity of the catalyst and used a Fourier-transform infrared (FTIR) gas analyzer (DX4000, Gasmet). The compositions of reaction gas were 1,000 μL/L NO, 1,000 μL/L NH_3, 4% O_2 and N_2 balanced. The total flow rate was 500 mL/min over 1 mL catalyst and the GHSV was also 30,000 h^{-1}. N_2 selectivity was calculated by the following formula:

$$S_{N_2} = \frac{[NO]_{in} + [NH_3]_{in} - 2[N_2O]_{out} - [NO_2]_{out}}{[NO]_{in} + [NH_3]_{in}} \times 100\% \quad (3)$$

To eliminate the errors caused by the ammonia oxidation, 98.5% strong phosphoric acid solution was installed at the upstream of the gas analyzer used as an ammonia trap. To ensure that the decrease of NO_x concentration was not caused by the absorption of the catalyst powder, the catalyst was purged by reactor gas. Not until there was no difference between the NO_x concentration of inlet and outlet of the reactor was the NH_3 supplied into the system.

3. Catalyst Characterization

X-ray diffraction patterns were obtained by an X-ray Diffraction Analyzer (Rigaku D/max 2500 PC diffractometer) with Cu K_α radiation. The data of 2θ from 10° to 90° were collected at 4°/min with the step size of 0.1°.

N_2 adsorption-desorption isotherm at −196 °C was measured on ASAP2020 surface area and porosity analyzer (Micromeritics Instrument Corporation, American). Prior to N_2 physisorption, the catalysts were degassed at 300 °C for 5 h. The specific surface areas were determined by using the Brunauer-Emmett-Teller (BET) equation, and the specific pore volumes, average pore diameters and pore size distributions were calculated by the Barrett-Joyner-Halenda (BJH) method.

Microstructure of the catalysts was characterized by a cold field emission scanning electron microscope (SEM, JSM-6700F, Japan). Qualitative and quantitative analysis of the surface elements of the catalysts were obtained by using an energy dispersive spectrometer (EDS, Be4-U92, Oxford INCA X sight, OIMS, UK).

RESULT AND DISCUSSION

1. SCR Activity

The NO_x conversion and N_2 selectivity of $Fe_{0.7}Mn_{0.15}Mg_{0.15}O_z$ catalyst were tested from 50 °C to 200 °C and compared with γ-Fe_2O_3 catalyst and other excellent low-temperature catalysts reported pre-

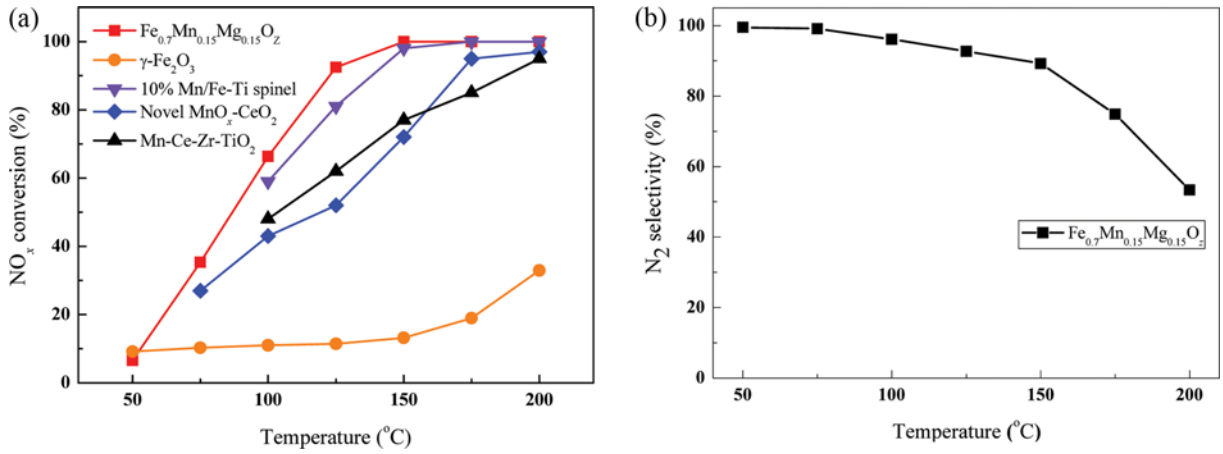

Fig. 1. (a) NO_x conversion in NH_3 SCR reaction over $Fe_{0.7}Mn_{0.15}Mg_{0.15}O_z$, γ-$Fe_2O_3$, 10% Mn/Fe-Ti spinel, MnO_x(20)/$Ce_{0.3}Zr_{0.7}O_2$(30)-TiO_2 and novel MnO_x-CeO_2 catalysts; (b) N_2 selectivity of $Fe_{0.7}Mn_{0.15}Mg_{0.15}O_z$ catalyst.

viously, as shown in Fig. 1. γ-Fe_2O_3 catalyst showed pool low-temperature SCR performance and nearly had no activity from 50 °C to 125 °C. Then with doping of manganese and magnesium, the performance of the catalyst was optimized greatly. By gradual increase in temperature, NO_x conversion catalyzed by $Fe_{0.7}Mn_{0.15}Mg_{0.15}O_z$ was increased until 150 °C, where the NO_x conversion achieved 100%, which was 85% higher than γ-Fe_2O_3 catalyst. NO_x conversion of $Fe_{0.7}Mn_{0.15}Mg_{0.15}O_z$ of 90% could be achieved over 125 °C. In addition, previous studies had reported the catalysts with prominent low-temperature activity. 10% Mn/Fe-Ti spinel [16], MnO_x(20)/$Ce_{0.3}Zr_{0.7}O_2$(30)-TiO_2 [17] and a novel MnO_x-CeO_2 catalyst with shell-in-shell microsphere structure [18] all showed excellent performance at low temperature. The maximum NO_x conversion could be reached at 175 °C, 200 °C and 200 °C, respectively. Compared with the catalysts mentioned above, $Fe_{0.7}Mn_{0.15}Mg_{0.15}O_z$ had higher NO_x conversion rate at lower reaction temperature. Besides that, the N_2 selectivity of $Fe_{0.7}Mn_{0.15}Mg_{0.15}O_z$ could maintain over 90% in the temperature range of 50-150 °C as illustrated in Fig. 1(b). Based on the NO_x conversion and N_2 selectivity, it could be concluded that manganese and magnesium elements were excellent compound dopants, and could significantly optimize the low-temperature SCR performance.

Furthermore, Yu [19] found that when metal elements were doped into catalysts as additives or active ingredients, the interaction among the metal elements would make better performance than the catalysts with single component. Chen [20] ascribed the superior SCR performance of CeO_2-WO_3 catalyst to the intense interactions between CeO_2 and WO_3. Combined with the XRD result following, it seemed that the intense interactions among iron, manganese and magnesium held the key to the optimization of low-temperature SCR performance.

2. Characterization Analysis

The comparative XRD patterns of γ-Fe_2O_3 and $Fe_{0.7}Mn_{0.15}Mg_{0.15}O_z$ catalysts are shown in Fig. 2, where both the samples presented sharp diffraction peaks for γ-Fe_2O_3 (JCPDS PDF #39-1346 2θ= 31°, 31°, 43°, 54°, 57°, 63°) and indicated the main components of γ-Fe_2O_3 with a good crystallinity in the two catalysts. The differences for $Fe_{0.7}Mn_{0.15}Mg_{0.15}O_z$ differing from the characteristic peaks

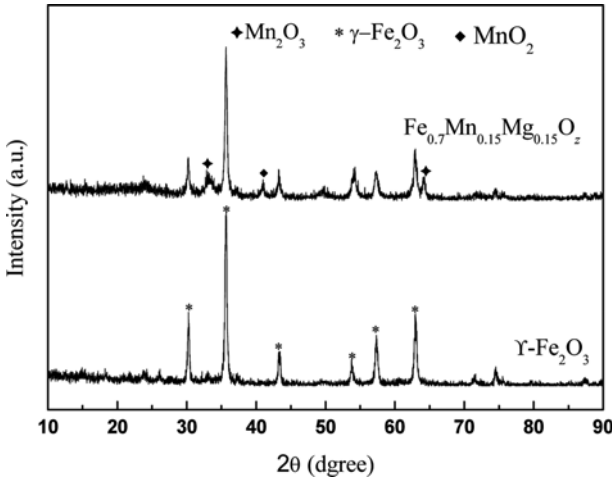

Fig. 2. XRD patterns of $Fe_{0.7}Mn_{0.15}Mg_{0.15}O_z$ and γ-Fe_2O_3 catalysts.

of γ-Fe_2O_3 belonged to the characteristic peaks of Mn_2O_3 (JCPDS PDF #89-4836 2θ=33°, 66°) and MnO_2 (JCPDS PDF #65-2821 2θ=41°). Furthermore, there was no characteristic peak of MgO_x. Thus, during the preparation of $Fe_{0.7}Mn_{0.15}Mg_{0.15}O_z$ catalyst, Mn_2O_3 and MnO_2 crystalline phases were generated and the Mg element had a high dispersity and poor crystallinity.

Comparing the two patterns, the diffraction peaks of $Fe_{0.7}Mn_{0.15}Mg_{0.15}O_z$ were lower and wider than those of γ-Fe_2O_3, which demonstrated the crystalline grains of $Fe_{0.7}Mn_{0.15}Mg_{0.15}O_z$ catalyst were smaller and more uniform. The introduction of magnesium and manganese consolidated the dispersity of γ-Fe_2O_3 and the magnesium and a part of manganese existed as an amorphous phase on the surface of catalyst. Thus, the interaction among the iron, manganese and magnesium species truly existed on the catalyst surface, which could lead to better dispersion. Shi [21] indicated that the active component with a high dispersity was beneficial to the low-temperature SCR. On the other hand, the rest of the manganese had excellent crystallinity and existed as MnO_2 and Mn_2O_3. According to the literature [12,22], SCR activity of MnO_x was connected with the type and crystallinity of MnO_x. MnO_2 showed the

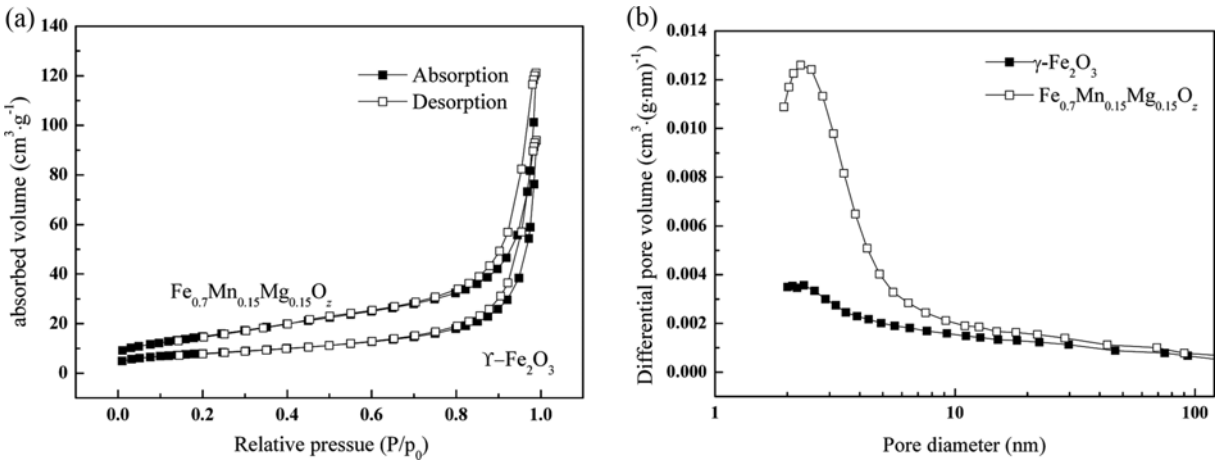

Fig. 3. (a) N_2 adsorption-desorption isotherms; (b) BJH desorption pore size distribution plots of γ-Fe_2O_3 and $Fe_{0.7}Mn_{0.15}Mg_{0.15}O_z$ catalysts.

optimal SCR performance and increased the low-temperature SCR performance remarkably. Therefore, with magnesium and manganese doped, the promotion on low-temperature SCR performance included two methods. For one thing, the doping of magnesium and manganese refined the crystalline grains, generated good solid solution and existed in an amorphous phase on the surface of catalysts. For the other, a part of manganese doped generated new crystalline phase, Mn_2O_3 and MnO_2, which had enormous promotion on the low-temperature SCR reaction. Comprehensively considering the two methods above, the $Fe_{0.7}Mn_{0.15}Mg_{0.15}O_z$ catalyst had a better low-temperature SCR performance than that of γ-Fe_2O_3 catalyst.

The SCR reaction rate was influenced by surface area, pore size and volume and the rates of absorption and desorption of the catalysts in microcosmic view. So, in order to reveal the promotion mechanisms of magnesium and manganese doped on the SCR reaction, N_2 adsorption-desorption tests were conducted. Fig. 3 and Table 1 show the results of N_2 adsorption-desorption tests for γ-Fe_2O_3 and $Fe_{0.7}Mn_{0.15}Mg_{0.15}O_z$ catalysts. In Table 1, the BET surface area and pore volume of $Fe_{0.7}Mn_{0.15}Mg_{0.15}O_z$ catalyst were, respectively, 1.9 times and 1.3 times bigger than those of γ-Fe_2O_3 catalyst. These results proved that doping magnesium and manganese elements could optimize the pore structure and increase the specific surface area and the specific pore volume, which could further confirm the existence of the interactions among the iron, manganese and magnesium. And the bigger surface area and pore volume indicated the better pore structure of $Fe_{0.7}Mn_{0.15}Mg_{0.15}O_z$ catalyst, which could decrease the resistance of the mass transfer process and ensure it in a considerable speed. After doping magnesium and manganese, the surface area and the pore volume of catalyst both increased. And because the SCR performance of catalysts was relative to the amount of active sites which were proportional to surface area and average pore volume [23], the $Fe_{0.7}Mn_{0.15}Mg_{0.15}O_z$ catalyst showed the better SCR performance.

Table 1. The structure properties of γ-Fe_2O_3 and $Fe_{0.7}Mn_{0.15}Mg_{0.15}O_z$ catalysts characterized by N_2 adsorption-desorption

Samples	S_{BET} ($m^2 \cdot g^{-1}$)	Pore volume ($cm^3 \cdot g^{-1}$)	Average pore diameter (nm)
γ-Fe_2O_3	27.93	0.147	21.2
$Fe_{0.7}Mn_{0.15}Mg_{0.15}O_z$	54.24	0.191	13.1

The porous structures and pore size distribution of the prepared samples are further demonstrated in Fig. 3. As shown in Fig. 3(a), the N_2 absorption-desorption isotherms of γ-Fe_2O_3 and $Fe_{0.7}Mn_{0.15}Mg_{0.15}O_z$ were both typical type V with H3 hysteresis loops according to the sorting method of International Union of Pure and Applied Chemistry (IUPAC) [24]. In the low pressure stage, the isotherms were gradual. The interactions between N_2 and the catalyst samples were fairly weak; furthermore, there was no N_2 absorbed. That indicated there were little micropores (<2 nm) in the samples. When the ratio of p/p_0 was over 0.8, the absorbed volume of N_2 increased rapidly. This was due to the existence of mesopores where the N_2 condensed and accumulated. Because the two samples both had H3 hysteresis loops, we inferred that there were many wedge-shaped pores incompactly accumulated by some sheet particles. Pore size distribution plots in Fig. 3(b) showed that interactions among the three ions of the $Fe_{0.7}Mn_{0.15}Mg_{0.15}O_z$ catalyst had increased the amount of mesopores (2-50 nm), especially the size from 2 to 6 μm. Therefore, the doping of manganese and magnesium had optimized the pore size distribution. In general, the micropores and the mesopores of the catalyst could provide biggest internal surface area and pore volume, while the macropores (>50 nm) were beneficial to the mass transfer process. Thus, optimized distribution and proportion of micropores, mesopores and macropores were significant reasons for the excellent SCR performance of $Fe_{0.7}Mn_{0.15}Mg_{0.15}O_z$ catalyst.

Fig. 4 shows SEM images of γ-Fe_2O_3 and $Fe_{0.7}Mn_{0.15}Mg_{0.15}O_z$ catalysts. From the images, it is seen that γ-Fe_2O_3 and $Fe_{0.7}Mn_{0.15}Mg_{0.15}O_z$ catalysts displayed different morphology in a microcosmic view. γ-Fe_2O_3 shows severe collapse and conglutination; consequently, the formation communication was awful. After manganese and magnesium doped, the morphology was remarkably optimized as shown in Fig. 3(b). The surface of $Fe_{0.7}Mn_{0.15}Mg_{0.15}O_z$ was looser and had many channels accumulated by the particles. Meanwhile, because the particles distributed independently and had less con-

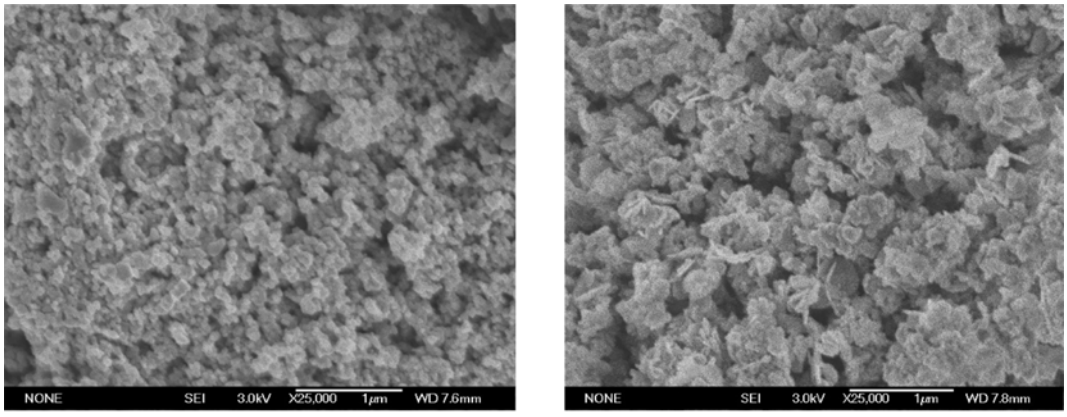

(a) (b)

Fig. 4. (a) SEM photo of γ-Fe_2O_3; (b) SEM photo of $Fe_{0.7}Mn_{0.15}Mg_{0.15}O_z$.

Table 2. EDS analysis data of γ-Fe_2O_3 and $Fe_{0.7}Mn_{0.15}Mg_{0.15}O_z$ catalysts

Catalyst	Percentage by weight (wt%)				Percentage by atomicity (at%)				O/Fe	
	Fe	O	Mn	Mg	Fe	O	Mn	Mg	Weight ratio	Atomicity ratio
γ-Fe_2O_3	68.19	31.81	-	-	38.05	61.95	-	-	0.47	1.63
$Fe_{0.7}Mn_{0.15}$-$Mg_{0.15}O_z$	53.04	38.20	5.17	3.59	26.54	66.71	2.63	4.13	0.72	2.51

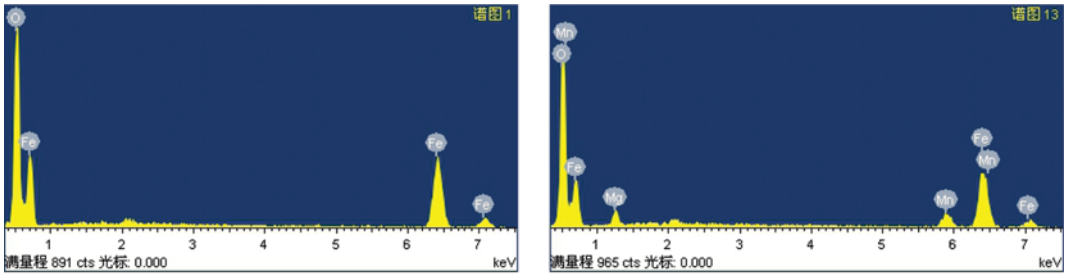

(a) (b)

Fig. 5. (a) EDS spectra of γ-Fe_2O_3; (b) EDS spectra of $Fe_{0.7}Mn_{0.15}Mg_{0.15}O_z$.

glutination, the sample appeared less collapse and better formation communication which could reduce the resistance of the mass transfer process. Therefore, the morphology in a microcosmic view of the catalysts was optimized by Mn and Mg elements.

Surface component analysis of the samples tested by EDS method is exhibited in Fig. 5. The main elements in the γ-Fe_2O_3 catalyst sample were Fe and O as shown in Fig. 5(a), while those were Fe, Mn, Mg and O in the $Fe_{0.7}Mn_{0.15}Mg_{0.15}O_z$ catalyst showed in Fig. 5(b). Therefore, the analysis results of EDS spectra of the two samples were the same as the expected active components.

From Table 2, the percentages by weight and atomicity of the catalysts surface elements were tested, and the weight and atomicity ratios of O/Fe on the surfaces of γ-Fe_2O_3 and $Fe_{0.7}Mn_{0.15}Mg_{0.15}O_z$ catalyst were obtained. From the data, the two catalysts' atomicity ratios of O/Fe were, respectively, 1.63 and 2.51. It indicated that more lattice oxygen existed on the surface of the $Fe_{0.7}Mn_{0.15}Mg_{0.15}O_z$ catalyst with the promotion of manganese and magnesium elements. Thus, abundant lattice and absorbed oxygen on the catalyst surface could increase the oxidation ability and the activity of the catalyst; furthermore, it would be beneficial to the SCR reaction.

3. Effect of NH_3

Fig. 6(a) presents the impacts of molar ratio of NH_3/NO on SCR activity of $Fe_{0.7}Mn_{0.15}Mg_{0.15}O_z$ with GHSV of 30,000/h at 125 °C. According to Langmuir-Hinshelwood mechanism and Eley-Rideal mechanism, NH_3 reacted with gas-phase NO after the absorption and activation of NH_3 on catalyst surface, and the gas-phase NH_3 showed little reactivity with NO in the gas-phase [25,26]. It could be learned from the SCR reaction formula that with the increase of NH_3 amount, the NH_3 absorbed on the catalyst was increased and promoted the NO_x conversion.

From Fig. 6(a), the NO_x conversion increased quickly as the molar ratio of NH_3/NO from 0 to 1. During the process, with the increase of the gas-phase NH_3, NH_3 absorbed and activated on unit area of catalyst at unit time got increased by a large margin and made a great promotion to NO_x conversion. However, when the molar ratio of NH_3/NO exceeded 1, NO_x conversion tended to

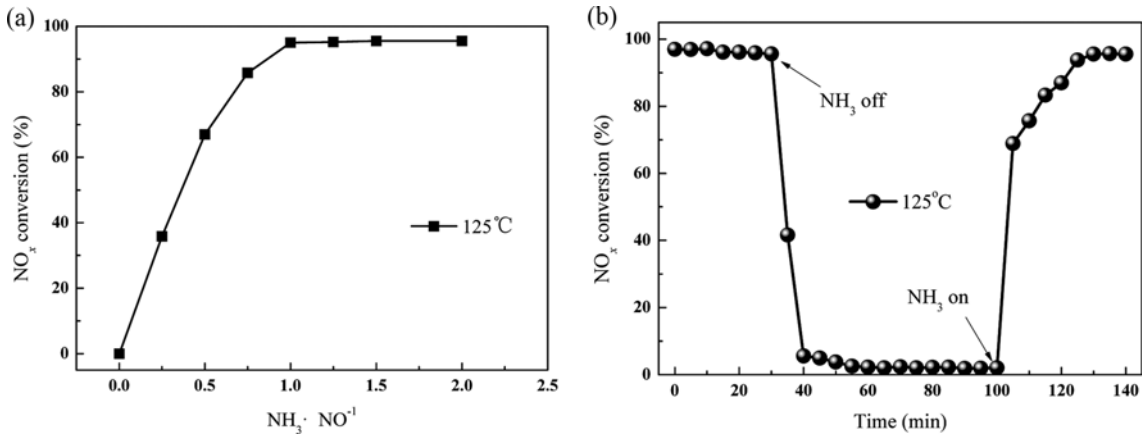

Fig. 6. (a) Effect of NH_3/NO concentration; (b) Transient response on $Fe_{0.7}Mn_{0.15}Mg_{0.15}O_z$ upon switching off and on NH_3. Reaction conditions: [NO]=1,000 μL/L, [O_2]=3.5%, balance N_2, total flow rate 2,000 mL/min, catalyst 4 mL, reaction temperature 125 °C.

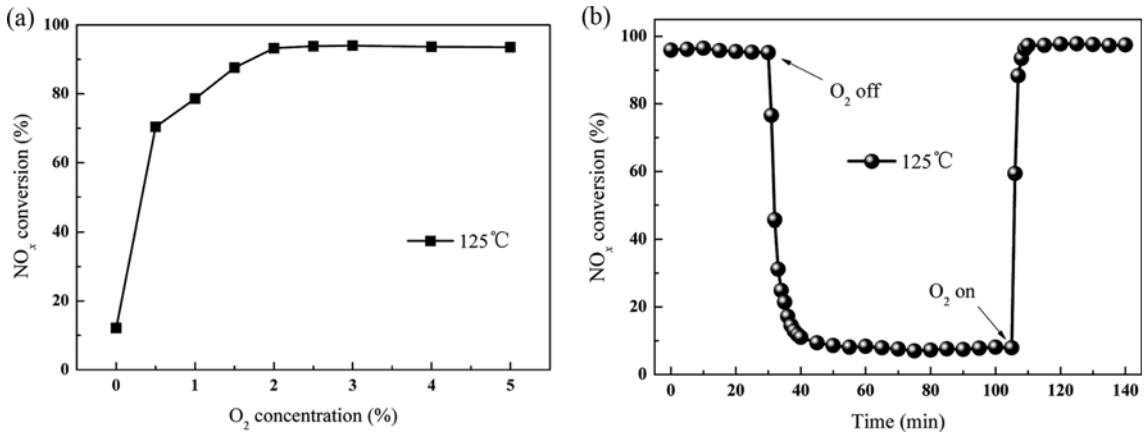

Fig. 7. (a) Effect of O_2 concentration; (b) Transient response on $Fe_{0.7}Mn_{0.15}Mg_{0.15}O_z$ upon switching off and on O_2. Reaction conditions: [NO]=[NH_3]=1,000 μL/L, balance N_2, total flow rate 2,000 mL/min, catalyst 4 mL, reaction temperature 125 °C.

show a constant value, which could be explained as that the absorbed sites were limited, and no more NH_3 could be absorbed on catalyst if NH_3 was excess. Considering the economic efficiency, excess NH_3 raised the operating cost, for the cost of NH_3 made up 25% of the operating cost of the SCR system [27]. And most importantly, it would make severe secondary pollution. Thus, the optimal molar ratio of NH_3/NO is 1.

The effect of NH_3 concentration on $Fe_{0.7}Mn_{0.15}Mg_{0.15}O_z$ catalyst could also be described in transient state. Under the operating condition mentioned above, transient behavior of the $Fe_{0.7}Mn_{0.15}Mg_{0.15}O_z$ was tested by switching NH_3 supply off and on in the flue gas, and the results are in Fig. 6(b). NO_x conversion declined quickly from 95.6% to 3.7% in the first 20 min, and then apparently achieved stability. Certain amount of nitrites and nitrates would be formed on the surface of the catalyst [28]. Therefore, without NH_3, the NO_x conversion would stay stable, as a result of the formation of nitrites and nitrates. Subsequently, after the reintroduction of NH_3, NO_x conversion was enhanced immediately. After the quick increment in the first 5 min, the increase of NO_x conversion became slow. This was because NH_3 participated in the reaction after being absorbed on the catalyst surface, and part of NH_3 would react with the nitrites and nitrates accumulated before [29]. Finally, NO_x conversion achieved and kept a stable state again 30 min after switching the NH_3 back on.

4. Effect of O_2

Numerous previous studies have proved the crucial effects of oxygen in SCR reaction [30]. Fig. 7(a) shows NO_x conversion profile of $Fe_{0.7}Mn_{0.15}Mg_{0.15}O_z$ vs O_2 concentration at 125 °C. $Fe_{0.7}Mn_{0.15}Mg_{0.15}O_z$ showed poor NO_x conversion of 12.1% in the absence of O_2 at 125 °C. It indicated that the oxygen participated in the SCR reaction at this moment was lattice oxygen and a little absorbed oxygen. However, when little O_2 was introduced, the NO_x conversion showed rapid enhancement. With O_2 concentration achieving 0.5%, the NO_x conversion quickly reached about 70.4% and was nearly 60% higher than that without O_2. Then with O_2 concentration further increasing, NO_x conversion of the catalyst increased slowly and peaked at 94% while the O_2 concentration reached 2% and subsequently remained invariable. The results demonstrated O_2 could participate in SCR reaction and play an important role in the SCR system [31,32].

The existence of O_2 could promote the NO oxidation to NO_2. And a high activity for NO oxidation to NO_2 could enhance the

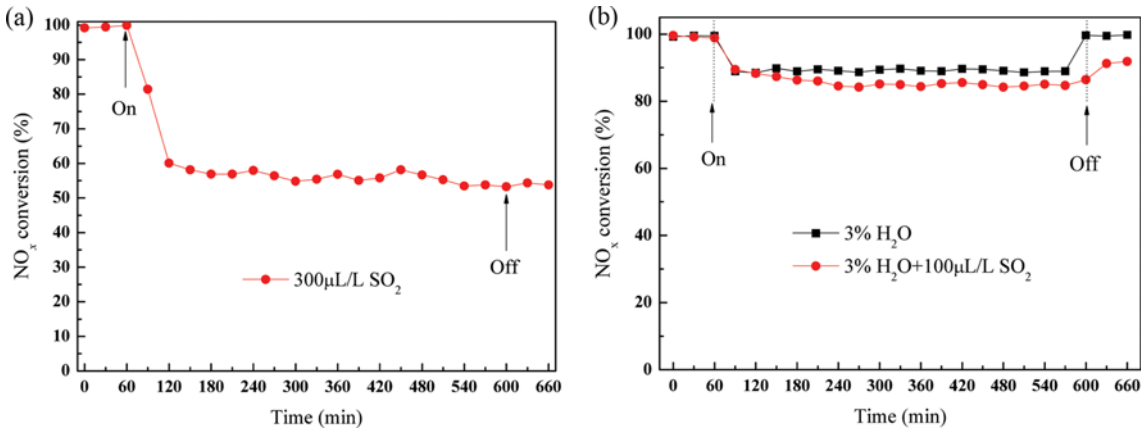

Fig. 8. (a) Effect of SO_2; (b) Effect of SO_2 and H_2O. Reaction conditions: [NO]=[NH_3]=1,000 μL/L, [O_2]=3.5%, balance N_2, total flow rate 2,000 mL/min, catalyst 4 mL, reaction temperature 150 °C.

SCR activity reported by Koebel [33] and Long [34]. Without O_2, there was only lattice oxygen and a little absorbed NO on the surface of the catalyst, by which time, only a tiny amount of NO participated in the SCR reaction and the SCR activity was low. When gas-phase O_2 was introduced, on the one hand, the gas-phase O_2 could accelerate SCR reaction by filling the oxygen vacancies [35] and promoting the absorption of NO; on the other hand, the addition of O_2 increased the amounts of absorbed oxygen on the catalyst surface which has been demonstrated to enhance SCR activity [36]. Moreover, according to the previous reports, chemisorbed oxygen was the most active oxygen and played an influential role in oxidation reaction [37]. Then while O_2 concentration exceeded 0.5%, especially 2%, the absorption capacity of O_2 achieved the maximum, after which the absorption and oxidation of NO gradually decreased. Xiong [38] showed that the NO_x conversion of iron-cerium mixed oxides catalyst was only 37.8% without O_2, then increased rapidly to 78.7% with the addition of O_2. When the O_2 concentration reached 0.5%, the increase of NO_x conversion slowed down. Therefore, O_2 played an important role in SCR reaction and only by keeping the O_2 concentration of 3%, could we guarantee the perfect SCR performance of the catalysts. In this paper, we chose the O_2 concentration of 3.5%.

To reveal the details of O_2 reaction process, transient behavior was tested in the same methods that NH_3 used and the results are shown in Fig. 7(b). As shown, when O_2 was turned off, there was a dramatic decline in NO_x conversion. After 40 min, NO_x conversion declined gradually and got a stable state 10 min later. The slow decrease indicated that O_2 absorbed on the catalyst surface was consumed gradually in the process. When NO_x conversion reached a stable state, it still appeared little conversion rate, which was about 10%. It could be explained that though O_2 was cut off at this moment, there was lattice oxygen on the catalyst and it was available for the reaction. When the O_2 was fed again, NO_x conversion increased rapidly caused by the quick restoration of the absorbed oxygen. Compared with the restoration rate of NO_x conversion in transient response experiment on NH_3, the restoration rate in O_2 transient response experiment was apparently quicker. According to this phenomenon, it could be inferred that O_2 could participate in the reaction at a faster rate than NH_3, which resulted from the difference that NH_3 participated in SCR reaction in absorbed state, while part of lattice oxygen took part in the reaction directly. Furthermore, it further verified the conclusion that when NH_3 was reintroduced, NH_3 would react with the nitrites and nitrates formed in the experiment besides the gas-phase and absorbed NO_x, which was obtained in the NH_3 transient response experiments. Finally, after the increase of NO_x conversion for a few minutes, the original efficiency of the SCR reaction was restored. Therefore, it was demonstrated that O_2 not only participated in the SCR reaction, but also had significant impacts on the reaction.

5. Effect of the Presence of H_2O and SO_2

H_2O and SO_2 contained in the flue gases usually led to a formation of sulfur compounds and caused a deactivation on SCR catalyst, so that it was of great significance to investigate the impacts of the presence of them. We knew that the flue gas temperature at downstream of desulfurization unit and electrostatic precipitator was about 150-160 °C [39], so the experiments were conducted at 150 °C and stabilized for 1 hour before the addition of H_2O and/or SO_2.

Fig. 8 illustrates the effects of H_2O and/or SO_2 on NO_x conversion of $Fe_{0.7}Mn_{0.15}Mg_{0.15}O_z$ catalyst and shows that in the absence of H_2O and SO_2, the steady NO_x conversion over $Fe_{0.7}Mn_{0.15}Mg_{0.15}O_z$ was nearly 100% at 150 °C. When 300 μL/L SO_2 was introduced, the NO_x conversion gradually decreased to 60% compared to the original 100% in 1 hour and then kept a stable value as shown in Fig. 8(a). It indicated that the deactivation of SO_2 was an accumulative and progressive process, which might be because many sulfates and/or sulfites formed on the surface of the catalyst blocked the active sites [40]. When SO_2 supply was removed, the activity of the catalyst did bot restore and still remained the same level. The phenomenon manifested that the inhibition effect of SO_2 was irreversible.

Fig. 8(b) shows that it exhibited a sharp decline to 88.8% after 3% H_2O added. And then it almost kept a stable state at this level. Furthermore, the NO_x conversion quickly restored to the original level with the supply of water vapor switched off. It showed the inhibitory effect of water vapor over $Fe_{0.7}Mn_{0.15}Mg_{0.15}O_z$ catalyst was reversible. This reversible effect was ascribed to the competing absorption of H_2O, which blocked the limited active sites for

the absorption of NO and NH_3 [41]. Moreover, the effect of SO_2 and H_2O was also shown in the graph. When 3% H_2O and 100 μL/L SO_2 were introduced into the reaction gas at 150 °C, the NO_x conversion decreased from nearly 100% to 84.5% gradually and then nearly kept stable. However, after the removal of SO_2 and H_2O, the NO_x conversion showed part restoration to about 91% and kept this level steadily. Compared with the inhibitory effect of H_2O alone, it was obvious that the inhibition in the coexistence of water vapor and SO_2 was cumulative and combinatorial. And the deactivation could be attributed to two aspects. On the one hand, the water vapor could enhance the amount of surface hydroxyl and facilitate the absorption of SO_2. On the other hand, water vapor changed the structure of sulfates and formed $(NH_4)_2SO_4$ and NH_4HSO_4 with NH_3, which could cover the active sites and block the pores of the catalyst [42]. While switching off the addition of water vapor and SO_2, however, the NO_x conversion showed little recovery, which indicated that the inhibitory effect was irreversible.

CONCLUSION

$Fe_{0.7}Mn_{0.15}Mg_{0.15}O_z$ catalyst showed high activity for low-temperature SCR of NO with NH_3, and 90% NO_x conversion of it could be achieved over 125 °C. According to the results of characterization tests, the doping of magnesium and manganese consolidated the dispersity of γ-Fe_2O_3. A part of manganese and magnesium existed as an amorphous phase and formed a solid solution with γ-Fe_2O_3 on the surface of catalyst. And the other manganese would be well crystallized as Mn_2O_3 and MnO_2. $Fe_{0.7}Mn_{0.15}Mg_{0.15}O_z$ catalyst had better pore structures and more excellent pore diameter distribution. Furthermore, after manganese and magnesium doping, the collapse and conglutination of the catalyst decreased. Meanwhile, the catalyst had better formation communication, which reduced the resistance of mass transfer process. In addition, the optimal O_2 concentration and molar ratio of NH_3/NO were 3% and 1, respectively. NH_3 participated in the SCR reaction in absorbed states, whereas O_2 took part in the reaction in gas phase directly. Thus, O_2 could participate in the reaction in a faster rate than NH_3. And the effect of SO_2 was proved to be irreversible, whereas the inhibition of H_2O could be rapidly removed after its removal.

ACKNOWLEDGEMENT

This work was financially supported by the National Natural Science Foundation of China (51276101, 51576117) and the Fundamental Research Funds of Shandong University (2015JC024).

REFERENCE

1. L. B. Duan, Y. Q. Duan and C. S. Zhao, *Fuel*, **150**, 8 (2015).
2. M. Kuang and Z. Q. Li, *Energy*, **59**, 144 (2014).
3. I. Nova, C. Ciardelli, E. Tronconi, D. Chatterjee and B. Bandl-Konrad, *Catal. Today*, **114**, 3 (2006).
4. J. H. Li, H. Z. Chang, L. Ma, J. M. Hao and R. T. Yang, *Catal. Today*, **175**, 147 (2011).
5. X. Tang, J. Hao, W. Xu and J. Li, *Catal. Commun.*, **8**, 329 (2007).
6. J. Li, J. Chen, R. Ke, C. Luo and J. Hao, *Catal. Commun.*, **8**, 1896 (2007).
7. F. D. Liu, H. He and C. B. Zhang, *Chem. Commun.*, **17**, 2043 (2008).
8. A. Kato, S. Matsuda, T. Kamo, F. Nakajima, H. Kuroda and T. Narita, *J. Phys. Chem.*, **85**, 4099 (1981).
9. H. Teng, L. Y. Hu and Y. C. Lai, *Environ. Sci. Technol.*, **35**, 2369 (2001).
10. G. Marbán and A. B. Fuertes, *Catal. Lett.*, **84**, 13 (2002).
11. D. A. Peña, B. S. Uphade and P. G. Smirniotis, *J. Catal.*, **221**, 421 (2004).
12. F. Kapteijn, L. Singoredjo and A. Andreini, *Appl. Catal.*, **3**, 173 (1994).
13. F. D. Liu, H. He, Y. Ding and C. B. Zhang, *Appl. Catal.*, **93**, 194 (2009).
14. B. X. Shen, Y. Yao, H. Q. Ma and T. Liu, *Chin. J. Catal.*, **32**, 1803 (2011).
15. L. Valanidou, C. Theologides, A. A. Zorpas, P. G. Sawa and C. N. Costa, *Appl. Catal. B. Environ.*, **107**, 164 (2011).
16. S. J. Yang, F. H. Qi, S. C. Xiong, H. Dang, Y. Liao, P. K. Wong and J. H. Li, *Appl. Catal.*, **181**, 570 (2016).
17. S. H. Jo, B. Shin, M. C. Shin, C. J. V. Tyne and H. Lee, *Catal. Commun.*, **57**, 134 (2014).
18. C. Liu, G. Gao, J. W. Shi, C. He, G. Li, N. Bai and C. Niu, *Catal. Commun.*, **86**, 36 (2016).
19. G. F. Yu, Y. F. Wei, R. B. Jin, H. Zhu, Z. Y. Gu and L. L. Pan, *Acta. Scien. Circum.*, **32**, 1743 (2012).
20. L. Chen, J. H. Li, W. Ablikim, J. Wang, H. Z. Chang, L. Ma, J. Y. Xu, M. F. Ge and H. Arandiyan, *Catal. Lett.*, **141**, 1859 (2011).
21. Y. N. Shi, S. Chen, H. Sun, Y. Shu and X. Quan, *Catal. Commun.*, **42**, 10 (2013).
22. D. Fang, J. L. Xie, H. Hu, H. Yang, F. He and Z. B. Fu, *Chem. Eng. J.*, **271**, 23 (2015).
23. H. Q. Ma, Y. Yao, J. Ma and B. X. Shen, *J. Eng. Therm.*, **34**, 164 (2013).
24. R. A. Pierotti, *J. Rouquérol. Pure Appl. Chem.*, **57**, 603 (1985).
25. G. Busca, L. Lietti, G. Ramis and F. Berti, *Appl. Catal. B. Environ.*, **18**, 1 (1998).
26. M. A. Larrubia, G. Ramis and G. Busca, *Catal. B. Environ.*, **30**, 101 (2001).
27. B. Guo, H. K. Liao, C. H. Xu and Y. J. Liao, *Therm. Pow. Eng.*, **25**, 437 (2010).
28. W. S. Kijlstra, D. S. Brands, H. I. Smit and E. K. Poels, *J. Catal.*, **171**, 219 (1997).
29. Z. B. Wu, B. Q. Jiang, Y. Liu, W. R. Zhao and B. H. Guan, *J. Hazard. Mater.*, **145**, 488 (2007).
30. H. Bosch and F. Janssen, *Catal. Today*, **2**, 369 (1988).
31. X. Gao, Y. Jiang, Y. Zhong, Z. Y. Luo and K. F. Cen, *J. Hazard. Mater.*, **174**, 734 (2010).
32. P. Balle, B. Geiger, D. Klukowsk, M. Pignatelli, S. Wohnrau, M. Menzei, I. Zirkwa, G. Brunklaus and S. Kuerti, *Appl. Catal. B*, **91**, 587 (2009).
33. M. Koebel, M. Elsener and G. Madia, *Chem. Res.*, **40**, 52 (2001).
34. R. Q. Long and R. T. J. Yang, *J. Catal.*, **198**, 20 (2001).
35. P. R. Ettireddy, N. Ettireddy, T. Boningari, R. Pardemann and P. G. Smirniotis, *J. Catal.*, **292**, 53 (2012).

36. Q. Y. Wu, J. X. Chen and J. Y. Zhang, *Fuel Process. Technol.*, **89**, 993 (2008).
37. Z. B. Wu, R. B. Jin, Y. Liu and H. Q. Wang, *Catal. Commun.*, **9**, 2217 (2008).
38. Z. B. Xiong, C. M. Lu, D. X. Guo, X. L. Zhang and K. H. Han, *J. Chem. Technol. Biotechnol.*, **88**, 1258 (2013).
39. G. S. Qi and R. T. Yang, *Appl. Catal. B. Environ.*, **44**, 217 (2003).
40. J. H. Li, H. Z. Chang, L. Ma, J. M. Hao and R. T. Yang, *Catal. Today*, **175**, 147 (2011).
41. M. D. Amiridis, I. E. Wachs, G. Deo, J. M. Jehng and D. S. Kim, *J. Catal.*, **161**, 247 (1996).
42. R. B. Jin, Y. Liu, Z. B. Wu, H. Q. Wang and T. T. Gu, *Catal. Today*, **153**, 84 (2010).